npj | 2D materials and applications

Article

Published in partnership with FCT NOVA with the support of E-MRS

https://doi.org/10.1038/s41699-024-00517-1

Theory of magnetotrion-polaritons in transition metal dichalcogenide monolayers

Andrejs Kudlis[1], Ivan Aleksandrov[2,3], Zaur Alisultanov[4,5], Kalman Varga[6], Ivan Shelykh[1] & Vanik Shahnazaryan[4,7]

Magnetic field is a powerful tool for the manipulation of material's electronic and optical properties. In the domain of transition metal dichalcogenide monolayers, it allows one to unveil the spin, valley, and orbital properties of many-body excitonic complexes. Here we study theoretically the impact of normal-to-plane magnetic field on trions and trion-polaritons. We demonstrate that spin and orbital effects of a magnetic field give comparable contributions to the trion energies. Moreover, as magnetic field redistributes the free electron gas between two valleys in the conductance band, the trion-photon coupling becomes polarization and valley dependent. This results in an effective giant Zeeman splitting of trion-polaritons, in-line with the recent experimental observations.

Monolayers of transition metal dichalcogenides (TMD) are representatives of the family of two-dimensional (2D) materials which reveal robust excitonic response. The corresponding bright exciton binding energies reach hundreds of meV[1], and the presence of tightly bound excitons with large optical oscillator strength determine the optical spectra of TMD monolayers up to room temperatures[2]. Moreover, in contrast to the case of conventional semiconductor quantum wells, excited excitonic states are clearly seen in the reflection spectrum[3]. They are characterized by non-Rydberg energy scaling resulting from the reduced screening of Coulomb interaction peculiar for a truly 2D system[4–7].

TMD monolayers have a hexagonal lattice structure with band edge minima at ± K points of the Brillouin zone forming two non-equivalent valleys characterized by opposite spin polarizations[8]. This gives rise to emergent spin-valley physics[9], which in the domain of excitonics is characterized by a large variety of exciton species[10], and determines the great potential of the considered materials for nanoscale device applications[11–13].

A direct consequence of tightly bound character of excitons in TMD monolayers is an ability to reach the regime of high density of excitons with $n \sim 10^{12}$–10^{13} cm^{-2} [14,15], which is orders of magnitude larger than in conventional 2D systems based on GaAs quantum wells[16]. In this regime the nonlinear optical effects associated with exciton-exciton Coulomb interactions become prominent[17–22]. Such nonlinear behavior is further enhanced in the presence of an optical microcavity, where the regime of strong light-matter coupling occurs and exciton-polaritons are formed[23].

Excitonic and polaritonic properties of TMD monolayers are strongly affected by the presence of free electron gas. The unintentional doping routinely appears during the fabrication process, and the density of excess electrons can be controlled via external gating field[24], which thus becomes a control parameter for tuning of the exciton resonance. Moreover, the presence of free charge carriers results in a formation of three-body charged excitonic complexes—trions, characterized by a new emergent peak below the excitonic line in the optical spectrum[25–28]. It should be noted that at high densities of free carriers the underlying physics of exciton-electron interaction becomes more complex, and a crossover from trions to repulsive (exciton) and attractive (trion) polarons occurs[29–32]. Yet, at low densities of itinerant electrons, the exciton-trion picture is sufficient for description of the optical response[33].

Similar to excitons, trions are efficiently coupled to light. The regime of strong light-matter coupling in microcavities with doped TMD monolayers is well elaborated[34,35]. Interestingly, the nonlinear response associated with trion polaritons is larger as compared to excitons[36,37], and can be further enhanced by means of an external magnetic field[38], which was also used to reveal the Rydberg series, and determine effective masses and g-factors of excitons[39–44]. However, the existing studies of the magnetic field impact on trions in TMD monolayers focus on a valley Zeeman splitting only[45,46] with orbital effects being typically neglected[33]. In this paper we thus develop a microscopic formalism where orbital and spin effects of a magnetic field are treated on equal footing, demonstrating that in the case of trions they give

[1]Science Institute, University of Iceland, Reykjavik, Iceland. [2]Department of Physics, Saint Petersburg State University, Saint Petersburg, Russia. [3]Ioffe Institute, Saint Petersburg, Russia. [4]Abrikosov Center for Theoretical Physics, Dolgoprudnyi, Russia. [5]Institute of Physics of DFRS, Russian Academy of Sciences, Makhachkala, Russia. [6]Department of Physics and Astronomy, Vanderbilt University, Nashville, TN, USA. [7]Department of Physics, ITMO University, St. Petersburg, Russia. e-mail: vanikshahnazaryan@gmail.com

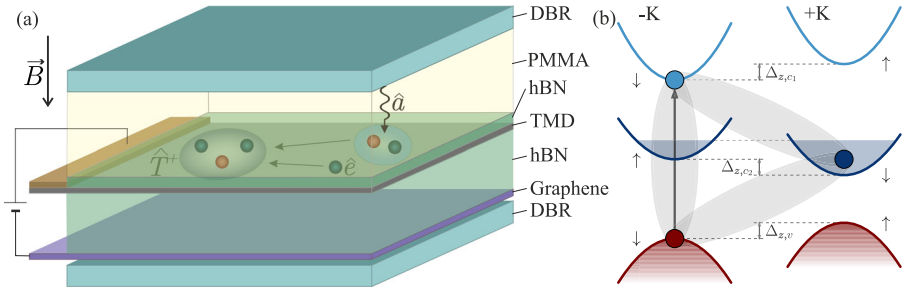

Fig. 1 | Schematic illustration of the considered system and the band structure of atomic monolayer. a Sketch of the structure. A hBN-encapsulated TMD monolayer hosting excess electrons is embedded in an optical microcavity in the presence of a normal-to-plane uniform magnetic field. The microcavity is filled with dielectric media represented by PMMA. A pair of electrodes consisting of a metallic gate and graphene layer is used to control the density of excess electrons. A cavity photon creates an electron-hole pair, which is associated with a free electron forming a three-particle bound state (a trion). The radiative recombination of a trion generates a cavity photon and a free electron. In high-Q optical cavity, a successive repetition of these processes leads to the onset of strong light-matter coupling regime and formation of hybrid states, trion-polaritons. **b** Band structure in the vicinity of ±K points of Brillouin zone and optical excitonic transition (thick arrow) in WSe_2 monolayer in the presence of free electron gas. The arrows indicate the subband's spin projection. The lowest-energy trion state in the -K valley is formed by an electron from the upper conduction subband and a hole from the upper valence subband, coupled with an excess electron, located in the +K valley of the lower conduction subband.

comparable contributions. We also demonstrate the vital role played by the mixing of different orbital channels.

Results and discussion

Trion states in the presence of a magnetic field

We consider the magnetic field impact on trion-polariton resonances in monolayer WSe_2, as schematically shown in Fig. 1a. The detailed description of the microscopic model is presented in the Methods section. The model takes into account band structure of the valleys near the ± K points of the Brillouin zone, as shown in Fig. 1b.

We start with addressing the exciton energy E_X defined as the ground state eigenvalue of electron-hole Hamiltonian in the absence of excess charge carriers. The exciton problem in a weak magnetic field is well studied[47], including the case of TMD monolayers[40–44]. The magnetic field results in a diamagnetic energy shift, which in the lowest order of perturbation theory amounts to $\Delta E_{\rm dia} \approx e^2\langle r^2\rangle B^2/8\mu$, where $\mu = \mu_{e1}\mu_h/(\mu_{e1}+\mu_h)$ is the exciton reduced mass, with μ_{e1}, μ_h denoting the effective masses of upper subband electron and a hole, respectively. The quantity $\langle r^2\rangle = \langle\psi_X|r^2|\psi_X\rangle$ is calculated in the absence of the magnetic field, where ψ_X is the wave function of exciton relative dynamics. To treat the problem more rigorously, we invoke the stochastic variational method (SVM). The numerical computation efficiency of the method greatly depends on the chosen trial function. Specifically, we use an ansatz of fully correlated two-dimensional Gaussians. The trial wave function is formed as a linear combination of these basis functions, optimized through random adjustments of parameters to minimize the ground state energy. Since the basis functions are not mutually orthogonal, we solve a generalized eigenvalue problem to find the energy levels and corresponding eigenvectors, providing variational upper bounds for the energies of the respective states. Further details of the model and computation scheme are presented in Methods section.

We employ two sets of basis functions. The first one includes a single orbital channel — $(m_e, m_h) = (0, 0)$, as in the case considered in ref. 48. The results of calculation are shown in Fig. 2a, b for monolayers WSe_2, and $MoSe_2$, respectively. The material parameters are given in Table 1. While in the absence of the magnetic field, the exciton binding energy is well reproduced, this approach demonstrates a linear (instead of quadratic) scaling with respect to the magnetic field, and severely overestimates the diamagnetic shift. On the contrary, by using the multi-orbital basis with the orbital channels $(0,0), (1,-1), (-1,1), (-2,2)$, and $(2,-2)$, one obtains the results which agree well with the experimental data and with the simple perturbative estimate discussed above.

We next numerically analyze the generalized eigenvalue problem defined by Eq. (11) of Methods for the trion states.

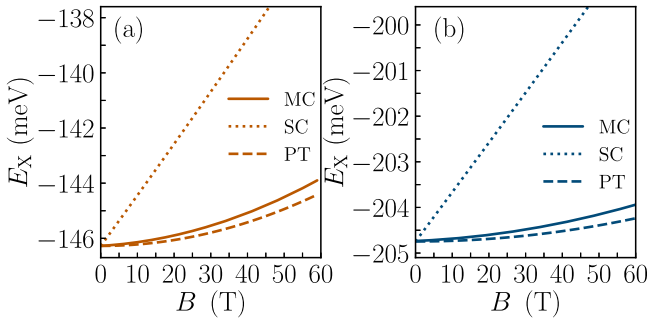

Fig. 2 | Magnetic field dependence of exciton energy. Exciton energy versus the magnetic field calculated for atomic monolayer **a** WSe_2, and **b** $MoSe_2$ by means of three different approaches. The dotted lines correspond to the single channel (SC) calculations within the SVM method, where one orbital channel $(m_e, m_h) = (0, 0)$ is taken into account as discussed in ref. 48. The resulting diamagnetic shift scales linearly with the magnetic field and is essentially larger compared to the experimental measurements. The dashed lines correspond to the calculation within perturbation theory (PT), where the diamagnetic shift is estimated via $\Delta E_{\rm dia} \approx e^2\langle r^2\rangle B^2/8\mu$, in accordance with the experimental results[40–44]. The solid lines show the SVM calculations of the exciton energy with a multi-orbital basis incorporating the following orbital channels: $(0,0), (1,-1), (-1,1), (-2,2)$, and $(2,-2)$.

We adopt the multi-orbital basis with all possible combinations $-2 \le m_i \le 2$ such that $\sum_i m_i = 0$. Such truncation of basis channels is enough for obtaining adequate precision of the calculation. We check the convergence of results expanding the basis to the case $-3 \le m_i \le 3$ [see Supplementary Note 1]. The results of the calculations are summarized in Fig. 3. In Fig. 3a we display the trion binding energy as a function of the magnetic field for various TMD monolayers. First of all, we note that the value of the trion binding energy in monolayer WSe_2 is above 20 meV in the absence of the magnetic field. Together with the exciton binding energy of $|E_X(\boldsymbol{B}=0)| = 146.3$ meV, this provides essentially better agreement with experimental data than the results reported in ref. 28. The larger value of the trion binding energy was obtained due to different effective masses of electrons in the spin subbands. The presence of a magnetic field leads to the increase of the trion binding energy, defined as

$$E_T^b = |E_X + \hbar\omega_e/2 - E_T|, \quad (1)$$

where E_T is the ground-state eigenvalue of Eq. (11), $\omega_e = e|\boldsymbol{B}|/\mu_{e2}$ is the cyclotron frequency of free electrons. The sublinear increase of trion binding

Table 1 | Characteristics of the materials considered in this work. Effective masses are taken from ref. 8, and screening lengths from ref. 41. Here E_b^X (E_b^T) is the calculated exciton (trion) binding energy in the absence of the magnetic field.

parameter	μ_{e1}	μ_{e2}	μ_h	κ	r_0	$\lvert E_X\rvert$	$\lvert E_T^b\rvert$
unit	m_0	m_0	m_0		nm	meV	meV
WSe_2	0.28	0.39	0.36	4.4	4.5	146.3	20.8
WS_2	0.26	0.35	0.36	4.4	3.4	162.8	23.5
$MoSe_2$	0.56	0.49	0.59	4.4	3.9	204.7	16.9
MoS_2	0.46	0.43	0.54	4.4	3.4	207.8	17.5

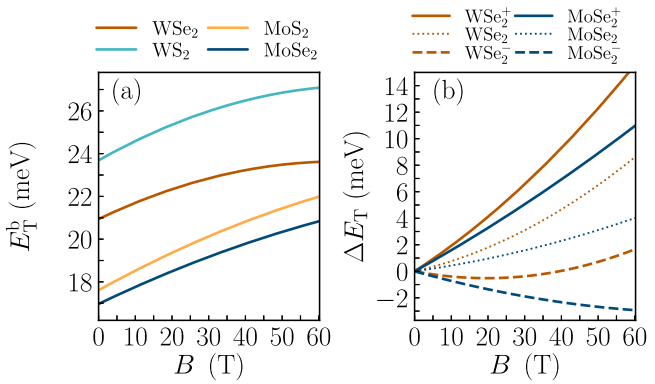

Fig. 3 | Magnetic field dependence of trion energy. a Trion binding energy versus the magnetic field, calculated using the expression (1) for various TMD monolayers. **b** Trion resonance energy shift as a function of the magnetic field for WSe_2 and $MoSe_2$ atomic monolayers. The dotted lines correspond to the diamagnetic shift. The solid and dashed lines demonstrate the total shift accounting for the Zeeman splitting for the two spin orientations.

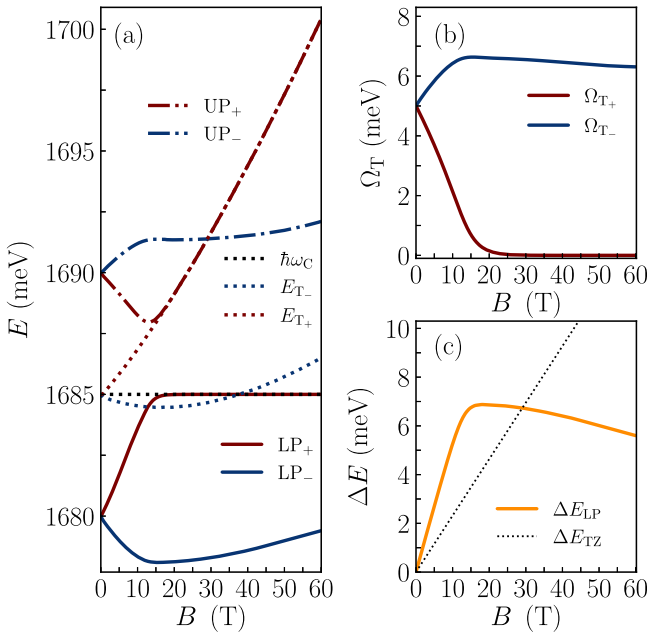

Fig. 4 | Magnetic field dependence of trion-polariton spectrum. a Energy of trion-polariton branches versus the magnetic field for atomic monolayer WSe_2. Red [blue] curves correspond $\sigma^{+[-]}$ circular polarizations. The increase of the magnetic field leads to a collapse of Rabi splitting for σ^+-polarized trions, and the respective increase of Rabi splitting for σ^--polarized trions. **b** Trion-photon coupling energy versus the magnetic field calculated via Eq. (26). **c** Zeeman splitting of bare trions (dotted line) and trion-polaritons (solid line). The reduction [enhancement] of Rabi splitting with increasing magnetic field for $\sigma^{+[-]}$-polarized results in a large increase of Zeeman splitting of trion-polaritons.

energy with increasing magnetic field is due to the competition of linear in magnetic field shift of free electron Landau level $\hbar\omega_e$, and the diamagnetic shift of trion eigenenergy E_T. We highlight that the suggested model adequately describes trion states at moderate density of free electron gas $E_F \ll E_T^b$[33]. Here E_F is the Fermi energy of free electron gas, defined in Methods.

In Fig. 3b the trion resonance energy shift versus magnetic field for monolayers of WSe_2 and $MoSe_2$ is shown. The pure diamagnetic shift defined as $\Delta E_T^{dia}(\boldsymbol{B}) = |E_T(\boldsymbol{B}) - E_T(\boldsymbol{B}=0)|$ is depicted by the dotted lines. We account for the magnetic field-induced Zeeman splitting of trion energy $\Delta E_{TZ} = g_X \mu_B B$[33], where μ_B is the Bohr magneton, $g_X = g_c - g_v$ is the exciton Lande factor defined via the Lande factors of upper conduction subband g_c, and valence band g_v[49]. The overall shift of trion resonances for the two spin orientations

$$\Delta E_T^{\pm}(B) = \Delta E_T^{dia}(B) \pm \Delta E_{TZ}/2 \quad (2)$$

is displayed in Fig. 3b by solid and dashed lines. Our direct calculations indicate that at the scale of 10 T of the applied magnetic field, the diamagnetic shift of the trion energy is comparable with the energy of Zeeman splitting.

Trion-photon coupling

We now consider the regime of strong light-matter coupling of trions with a near-resonant cavity eigenmode characterized by Eq. (29) of Methods. The negative trion resonance in hBN-encapsulated WSe_2 in the absence of the magnetic field and at low density of free carriers corresponds to $E_T^0 = 1685$ meV[28]. We use this value to choose the resonance energy of a cavity mode according to $\hbar\omega_C = E_T^0$. The dielectric constant of the media is set $\varepsilon = 3$, typical for PMMA[50], and the cavity length is found from the resonance condition in the form $L_C = 2\pi c/(\sqrt{\varepsilon}\omega_C)$, where c is the speed of light. We set the density of excess electrons at $n_e = 2\times10^{11}$ cm^{-2}, and also set $T = 4$ K. The dipole matrix element of the interband transition is chosen as $d_{cv} = 18$ Deb, resulting in $\Omega_T \approx 5$ meV in the absence of the magnetic field, typical for the trion-photon coupling[36,38,51].

The polarization-resolved magnetic field dependence of the polariton energies

$$E_T^{LP\pm} = \left(E_T^{\pm} + \hbar\omega_C^{\pm} - \sqrt{\left(2\Omega_T^{\pm}\right)^2 + \left(E_T^{\pm} - \hbar\omega_C^{\pm}\right)^2}\right)/2, \quad (3)$$

$$E_T^{UP\pm} = \left(E_T^{\pm} + \hbar\omega_C^{\pm} + \sqrt{\left(2\Omega_T^{\pm}\right)^2 + \left(E_T^{\pm} - \hbar\omega_C^{\pm}\right)^2}\right)/2 \quad (4)$$

for monolayer WSe_2 is shown in Fig. 4a. The σ^+ and σ^- polarized branches demonstrate the opposite behavior with increasing magnetic field: the Rabi splitting of the former reduces, while for the latter it increases. The reason is as follows. The magnetic field results in an imbalance of excess electrons, where a major part of them is transfered into +K valley, see Eq. (18) of Methods. As the trion photon-coupling rate scales as $\Omega_T \propto \sqrt{n_e}$, this gives rise to the reduction of trion-photon coupling for σ^+ polarization, and enhancement for σ^- polarization, as shown in Fig. 4b. The electron gas becomes fully polarized around 20 T of applied magnetic field, resulting in complete suppression of the trion-photon coupling for σ^+ polarization. We note here that the trion-photon coupling Ω_T depends on the magnetic field via the factor I_T as well, defined via the trion wave function, see Eq. (23). This particularly results in a minor reduction of trion-photon coupling at elevated values of magnetic field, as depicted in Fig. 4b.

The valley-dependent nature of the trion-photon coupling Ω_T in the presence of a magnetic field results in drastic modulation of the trion Zeeman splitting. As the lower trion-polariton energies of the two

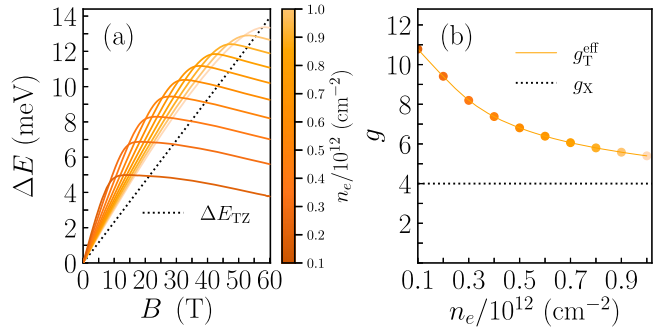

Fig. 5 | Renormalized Zeeman splitting. a Zeeman splitting of bare trions (black dotted line) and trion-polaritons for different values of free carrier density indicated on the color bar (solid orange curves). **b** Dependence of effective $g_T^{eff} = \Delta E_T^{LP}(B)/(\mu_B B)$ at $B \to 0$ on the free electron density n_e. The orange dots of varying color correspond to lines on the (**a**), and black dotted line indicates the bare g-factor $g_X = 4$.

polarizations shift in opposite directions with increasing magnetic field, in the strong-coupling regime, the effective Zeeman splitting $\Delta E_T^{LP} = E_T^{LP+} - E_T^{LP-}$ essentially increases, as shown in Fig. 4c. This result agrees well with a recent experimental observation of giant Zeeman splitting of trion-polaritons in $MoSe_2$-based structure[38]. The saturating character of effective Zeeman splitting at large magnetic field is due to complete polarizaion of the free electron gas. We note that the enhanced trion-polariton Zeeman splitting will result in respective circular polarization of photoluminescence spectra[52].

The spectra of WSe_2 atomic monolayer is characterized by two trion peaks, attributed to intravalley and intervalley trions[28]. While this additional trion peak has considerably smaller oscillator strength[53], its presence in the strong light-matter coupling Hamiltonian can modify the effective Zeeman splitting of lower trion-polariton branch (see Supplementary Note 2 for the details).

We next consider the impact of free electron gas density on trion-polariton effective Zeeman splitting. Generally the variation of free electron gas density affects the trion states via the additional screening of Coulomb interaction, and the Pauli blocking effects, resulting in slight modulation of trion wave function and spectral position[32,35,54]. Here we neglect this effect, assuming that the free electron gas density primarily affects the trion-photon coupling as $\Omega_T \propto \sqrt{n_e}$, see Eq. (26) in Methods. The trion-polariton effective Zeeman splitting for varying free electron gas density is depicted in Fig. 5a. The magnetic field-induced free electron valley polarization rate is defined via the ratio $\Delta E_{TZ}(B)/E_F^0$, see Eqs. (18), (17) in Methods. Hence, for smaller density n_e the complete valley polarization occurs at smaller magnetic field, as shown in Fig. 5a. One should note, however, that the further reduction of free electron gas density will result in the collapse of strong coupling regime between trion and photon states.

The renormalization of trion Zeeman splitting in strong light-matter coupling regime can be further quantified via an effective g-factor, defined as $g_T^{eff} = \Delta E_T^{LP}(B)/(\mu_B B)$ at $B \to 0$. At moderate density of free electrons $n_e = 10^{11}$ cm^{-2} one has $g_T^{eff} = 10.78$, about three times larger as compared to $g_X = 4$[49]. The modulation of g_T^{eff} with varying free electron gas density is shown in Fig. 5b.

Discussion

We developed a microscopic formalism for the description of magneto-trions and magnetotrion-polaritons in TMD monolayers. The spin and orbital effects of the magnetic field were treated on the same footing, and it was demonstrated that they give comparable contributions to the trion energy. We also showed that if a trion resonance is coupled to an optical cavity mode, the Zeeman splitting in the conductance band leads to a strong valley and polarization dependence of the trion-polariton energies, ultimately resulting in an effective giant Zeeman splitting for trion-polaritons.

Methods

Trion states in the presence of a magnetic field

We consider a trion state in the presence of a normal-to-plane uniform magnetic field $\boldsymbol{B}$ in monolayer WSe_2 placed inside a planar optical cavity represented by a pair of distributed Bragg reflectors (DBR), as shown in Fig. 1a. The excess electrons are located in the lowest spin split subband in the vicinity of K point of Brillouin zone, whereas an optical interband transition occurs to the upper subband (see Fig. 1b). This separation allows one to discard the phase space filling effects associated with Pauli blocking[33]. The Hamiltonian of a three-particle system consisting of two electrons with coordinates $\boldsymbol{r}_{1,2}$ and a hole with coordinate $\boldsymbol{r}_h$ is given by

$$\hat{H}_T = \hat{H}_{kin} + \hat{V}_{eh} + \hat{V}_{ee}, \tag{5}$$

where

$$\hat{H}_{kin} = \frac{\hat{\boldsymbol{\pi}}_1^2}{2\mu_{e1}} + \frac{\hat{\boldsymbol{\pi}}_2^2}{2\mu_{e2}} + \frac{\hat{\boldsymbol{\pi}}_h^2}{2\mu_h}, \tag{6}$$

$$\hat{V}_{eh} = -\sum_{j=1,2} V(|\boldsymbol{r}_j - \boldsymbol{r}_h|), \tag{7}$$

$$\hat{V}_{ee} = V(|\boldsymbol{r}_1 - \boldsymbol{r}_2|). \tag{8}$$

Here the momenta operators read $\hat{\boldsymbol{\pi}}_j = -i\hbar\nabla_j + e\boldsymbol{A}(\boldsymbol{r}_j)$, $\hat{\boldsymbol{\pi}}_h = -i\hbar\nabla_h - e\boldsymbol{A}(\boldsymbol{r}_h)$, e is the positive unit charge, and $\boldsymbol{A}$ is the vector gauge potential, $\nabla \times \boldsymbol{A} = \boldsymbol{B}$. The parameters $\mu_{e1}, \mu_{e2}, \mu_h$ are the effective masses of upper and lower subband electron, and a hole, respectively. The Coulomb interaction between charge carriers can be described by means of the Rytova-Keldysh potential[4,5]:

$$V(r) = \frac{e^2}{4\pi\varepsilon_0}\frac{\pi}{2r_0}\left[H_0\left(\frac{\kappa r}{r_0}\right) - Y_0\left(\frac{\kappa r}{r_0}\right)\right], \tag{9}$$

where ε_0 is the static dielectric constant, r_0 is the effective screening length, κ is the effective dielectric permittivity of surrounding media represented by a hexagonal boron nitride (hBN). H_0 and Y_0 are the Struve function and Bessel function of the second kind, respectively.

We employ a variational approach for the calculation of the ground state energy and wave function of the bound state. The numerical efficiency of the method strongly depends on the type of a trial function. The possible choice is the use of the anzats of fully correlated two-dimensional Gaussians[55,56]:

$$\Phi_{MS}^n(\boldsymbol{r}) = \mathcal{A}\left\{\left[\prod_{k=1}^{3}(x_k + iy_k)^{m_k^n}\right]\exp\left[-\frac{1}{2}\sum_{i,j=1}^{3}A_{ij}^n \boldsymbol{r}_i \boldsymbol{r}_j\right]\chi_{SM_S}\right\}, \tag{10}$$

where $\mathcal{A}$ is the antisymmetrization operator, $\boldsymbol{r} = (\boldsymbol{r}_1, \boldsymbol{r}_2, \boldsymbol{r}_3)$, the superindex $M = (m_1, m_2, m_3)$, χ_{SM_S} are linear combinations of single-particle spin functions corresponding to a given spin S and spin projection M_S. Throughout the paper we assume $\boldsymbol{r}_3 \equiv \boldsymbol{r}_h$.

The basis functions (10) are used to construct a trial wave function as a linear combination $\Psi = \sum_i c_i \Phi_i$, where the superindex i carries information about the orbital and spin quantum numbers. The functions Φ_i should be optimized within the procedure of random parameter modification in order to minimize the ground state energy. Given that these functions are not orthogonal to each other, one has to solve a generalized eigenvalue problem:

$$\sum_j \left(H_{ij} - EO_{ij}\right)c_j = 0, \tag{11}$$

$$H_{ij} = \langle\Phi_i|\hat{H}_T|\Phi_j\rangle, \quad O_{ij} = \langle\Phi_i|\Phi_j\rangle, \tag{12}$$

where as the output we obtain $E_1, E_2, E_3, \ldots$ as variational upper bounds of energies of respective states and corresponding eigenvectors. In what follows

we denote the trion ground state by $\Psi_T(\boldsymbol{r}_1, \boldsymbol{r}_2, \boldsymbol{r}_3)$. We perform a similar procedure for the exciton problem, where the ground-state wave function will be denoted by $\Psi_X(\boldsymbol{r}_1, \boldsymbol{r}_2)$.

The parameters of matrix A_{ij}^n can be found by means of the SVM method, which has proven its high efficiency in typical eigenvalue problems for few-body systems[57–60]. Detailed description of the numerical procedure is presented in refs. 48,55,56,61. Here we use the *svm-2d* package[55], in which we recalculate the matrix elements of the interparticle interaction with the potential (9) by Gauss-Legendre quadrature. We first make sure that in the absence of the magnetic field, the resulting trion binding energy matches with the previous reports[61]. As we only consider the ground state, we set for an exciton $S = 0$, $M_S = 0$, and for a trion $S = 1/2$, $M_S = 1/2$.

Valley distribution of free electron gas

No magnetic field. In the absence of magnetic field the density of states for each valley is $D_{\pm}(E) = \mu_{e2}/(2\pi\hbar^2)$, and the electron density

$$n_{e,\pm\mathrm{K}} = \frac{n_e}{2} = \frac{\mu_{e2}}{2\pi\hbar^2} k_\mathrm{B} T \log\left[\exp\left(\frac{E_\mathrm{F}^0}{k_\mathrm{B} T}\right) + 1\right]. \tag{13}$$

Here E_F^0 is the being the Fermi energy in the absence of the magnetic field, k_B denotes the Boltzmann constant, and T stands for the temperature. At the limit $E_\mathrm{F}^0 \gg k_\mathrm{B} T$ one has

$$n_{\mathrm{e},\pm\mathrm{K}} = \frac{n_\mathrm{e}}{2} = \frac{\mu_{e2}}{2\pi\hbar^2} E_\mathrm{F}^0, \tag{14}$$

yielding in $E_\mathrm{F}^0 = \pi\hbar^2 n_e/\mu_{e2}$.

Magnetic field impact. We consider the impact of magnetic field accounting for the valley Zeeman splitting of the lower conduction subband $\Delta E_{Z,c2} = g_{c2}\mu_\mathrm{B} B$, where g_{c2} is the Lande factor of the lower conduction subband. For the sake of simplicity we discard the formation of Landau levels and the respective modulation of 2D electron gas density of states, which can lead to some quantitative modification of the results. To obtain the Fermi energy dependence on magnetic field, the following conditions must be satisfied: (i) $n_{e,+\mathrm{K}} + n_{e,-\mathrm{K}} = n_e = \mathrm{const}$, (ii) $E_\mathrm{F}^- = E_\mathrm{F}^+ = E_\mathrm{F}$, (iii) $n_{e,\pm\mathrm{K}} \geq 0$. One has

$$\begin{aligned} n_e &= n_{e,+\mathrm{K}} + n_{e,-\mathrm{K}} \\ &= \int_{-\Delta E_{Z,c2}/2}^{\infty} \frac{\mu_{e2}}{2\pi\hbar^2} \frac{1}{\exp\left(\frac{E-E_\mathrm{F}}{k_\mathrm{B}T}\right)+1} \mathrm{d}E + \int_{\Delta E_{Z,c2}/2}^{\infty} \frac{\mu_{e2}}{2\pi\hbar^2} \frac{1}{\exp\left(\frac{E-E_\mathrm{F}}{k_\mathrm{B}T}\right)+1} \mathrm{d}E, \end{aligned} \tag{15}$$

yielding in

$$\begin{aligned} 2E_\mathrm{F}^0 = {} & k_\mathrm{B} T \log\left[\exp\left(\frac{E_\mathrm{F}+\Delta E_{Z,c2}/2}{k_\mathrm{B} T}\right) + 1\right] \\ & + k_\mathrm{B} T \log\left[\exp\left(\frac{E_\mathrm{F}-\Delta E_{Z,c2}/2}{k_\mathrm{B} T}\right) + 1\right]. \end{aligned} \tag{16}$$

Solving with respect to Fermi energy E_F, we get

$$\begin{aligned} E_\mathrm{F} = k_\mathrm{B} T \log\Bigg[& \sqrt{\exp\left(\frac{2E_\mathrm{F}^0}{k_\mathrm{B} T}\right) + \left(\cosh\left(\frac{\Delta E_{Z,c2}}{2k_\mathrm{B} T}\right)\right)^2 - 1} \\ & - \cosh\left(\frac{\Delta E_{Z,c2}}{2k_\mathrm{B} T}\right)\Bigg]. \end{aligned} \tag{17}$$

The electron densities in two valleys then read

$$n_{e,\pm\mathrm{K}} = \frac{n_e}{2} \frac{k_\mathrm{B} T}{E_\mathrm{F}^0} \log\left[\exp\left(\frac{E_\mathrm{F} \pm \Delta E_{Z,c2}/2}{k_\mathrm{B} T}\right) + 1\right]. \tag{18}$$

Trion-photon coupling

We consider a direct interband optical transition within a two-band approximation. We consider the case of the normal incidence, so that the photon wave vector $\boldsymbol{q}_\mathrm{ph} = 0$. The corresponding Hamiltonian can be represented as

$$\hat{\mathcal{H}}_\mathrm{rad} = \Omega \sum_{\boldsymbol{k}_e, \boldsymbol{k}_h} \left(\hat{a}_{\boldsymbol{k}_e}^\dagger \hat{b}_{\boldsymbol{k}_h}^\dagger + \hat{b}_{\boldsymbol{k}_h} \hat{a}_{\boldsymbol{k}_e}\right) \delta_{\boldsymbol{k}_e + \boldsymbol{k}_h, 0} \tag{19}$$

with

$$\Omega = d_{cv} \sqrt{\frac{\hbar\omega_\mathrm{C}}{2\varepsilon\varepsilon_0 L_\mathrm{C} S}}, \tag{20}$$

where ω_C is the cavity eigenfrequency, ε is the dielectric constant of a media typically represented by an organic polymer, such as polymethyl methacrylate (PMMA)[62–64]. Then L_C and S are the cavity length and sample area, respectively, d_{cv} is the dipole matrix element of the interband transition, $\hat{a}_{\boldsymbol{k}_e}^\dagger$, $\hat{b}_{\boldsymbol{k}_h}^\dagger$ are the creation operators for electrons and holes, respectively. The trion state can be expressed in the form

$$|T\rangle = \sum_{\boldsymbol{k}_1, \boldsymbol{k}_2, \boldsymbol{k}_h} F_\mathrm{T}(\boldsymbol{k}_1, \boldsymbol{k}_2, \boldsymbol{k}_h) \hat{a}_{\boldsymbol{k}_1}^\dagger \hat{\tilde{a}}_{\boldsymbol{k}_2}^\dagger \hat{b}_{\boldsymbol{k}_h}^\dagger |\phi\rangle, \tag{21}$$

where $\hat{\tilde{a}}_{\boldsymbol{k}_2}^\dagger$ corresponds to excess electrons, and $F_\mathrm{T}(\boldsymbol{k}_1, \boldsymbol{k}_2, \boldsymbol{k}_h)$ is the trion wave function in the momentum space. Accordingly, the excess electron state is $|e\rangle = \hat{\tilde{a}}_{\boldsymbol{k}}^\dagger |\phi\rangle$.

The coupling rate is then evaluated via

$$\begin{aligned} \langle T|\hat{\mathcal{H}}_\mathrm{rad}|e\rangle = {} & \Omega \sum_{\boldsymbol{k}_1, \boldsymbol{k}_2, \boldsymbol{k}_h} \sum_{\boldsymbol{k}_e', \boldsymbol{k}_h'} F_\mathrm{T}^*(\boldsymbol{k}_1, \boldsymbol{k}_2, \boldsymbol{k}_h) \delta_{\boldsymbol{k}_e' + \boldsymbol{k}_h', 0} \\ & \langle\phi|\hat{b}_{\boldsymbol{k}_h} \hat{\tilde{a}}_{\boldsymbol{k}_2} \hat{a}_{\boldsymbol{k}_1} \left(\hat{a}_{\boldsymbol{k}_e'}^\dagger \hat{b}_{\boldsymbol{k}_h'}^\dagger + \hat{b}_{\boldsymbol{k}_h'} \hat{a}_{\boldsymbol{k}_e'}\right) \hat{\tilde{a}}_{\boldsymbol{k}}^\dagger |\phi\rangle \\ = {} & \Omega \sum_{\boldsymbol{k}_h} F_\mathrm{T}^*(-\boldsymbol{k}_h, \boldsymbol{k}, \boldsymbol{k}_h) = \Omega I_\mathrm{T}(\boldsymbol{k}). \end{aligned} \tag{22}$$

In the presence of a magnetic field, the center-of-mass dynamics of trions cannot be straightforwardly decoupled from its internal dynamics, and one obtains

$$\begin{aligned} I_\mathrm{T}(\boldsymbol{k}) = {} & \sum_{\boldsymbol{k}_h} F_\mathrm{T}^*(-\boldsymbol{k}_h, \boldsymbol{k}, \boldsymbol{k}_h) \\ = {} & \frac{S}{(2\pi)^2} \frac{1}{S^{\frac{3}{2}}} \int \mathrm{d}^2\boldsymbol{k}_h \mathrm{d}^2\boldsymbol{r}_1 \mathrm{d}^2\boldsymbol{r}_2 \mathrm{d}^2\boldsymbol{r}_h e^{-i\boldsymbol{k}_h \boldsymbol{r}_1} e^{i\boldsymbol{k}\boldsymbol{r}_2} e^{i\boldsymbol{k}_h \boldsymbol{r}_h} \\ & \times \Psi_\mathrm{T}(\boldsymbol{r}_1, \boldsymbol{r}_2, \boldsymbol{r}_h) = \frac{1}{\sqrt{S}} \int \mathrm{d}^2\boldsymbol{r}_2 \mathrm{d}^2\boldsymbol{r}_h e^{i\boldsymbol{k}\boldsymbol{r}_2} \Psi_\mathrm{T}(\boldsymbol{r}_h, \boldsymbol{r}_2, \boldsymbol{r}_h). \end{aligned} \tag{23}$$

For the case of moderate dopings $|\boldsymbol{k}| \sim |\boldsymbol{k}_F| \ll a_\mathrm{tr}^{-1}$, where $a_\mathrm{tr} = \langle\Psi_\mathrm{T}|r|\Psi_\mathrm{T}\rangle$ is the effective Bohr radius of trion, and $\boldsymbol{k}_F \propto \sqrt{n_e}$ is the Fermi wave vector defined by excess electron density n_e. Hence, one can assume $e^{i\boldsymbol{k}\boldsymbol{r}} \approx 1$, so that $I_\mathrm{T}(\boldsymbol{k}) \approx I_\mathrm{T} = \mathrm{const}$[33].

We further introduce quasi-bosonic operators[36]

$$\hat{T}_\pm^\dagger = \frac{1}{\sqrt{N_{e,\pm\mathrm{K}}}} \sum_{\boldsymbol{k}} \hat{T}_{\boldsymbol{k}}^\dagger \hat{\tilde{a}}_{\boldsymbol{k}}, \tag{24}$$

where $N_{e,\pm\mathrm{K}} = n_{e,\pm\mathrm{K}} S$ is the total number of excess electrons in each valley. Then we find

$$\hat{H}_\mathrm{TC}^\pm = \Omega I_T \sqrt{N_{e,\pm\mathrm{K}}} \left(\hat{T}_\pm^\dagger \hat{c} + \hat{c}^\dagger \hat{T}_\pm\right) = \Omega_\mathrm{T}^\pm \left(\hat{T}_\pm^\dagger \hat{c} + \hat{c}^\dagger \hat{T}_\pm\right), \tag{25}$$

where

$$\Omega_{\mathrm{T}}^{\pm} = \sqrt{n_{e,\pm\mathrm{K}}}\Omega \int \mathrm{d}^2\boldsymbol{r}_2 \mathrm{d}^2\boldsymbol{r}_h \Psi_{\mathrm{T}}(\boldsymbol{r}_h, \boldsymbol{r}_2, \boldsymbol{r}_h). \tag{26}$$

In the absence of the magnetic field, the trion wave function can be factorized as $\Psi_{\mathrm{T}}(\boldsymbol{r}_1, \boldsymbol{r}_2, \boldsymbol{r}_h)|_{\boldsymbol{B}=0} = \psi_{\mathrm{T}}(\boldsymbol{r}_1 - \boldsymbol{r}_h, \boldsymbol{r}_2 - \boldsymbol{r}_h)/\sqrt{S}$, where ψ_{T} is the wave function of relative dynamics, and the center-of-mass dynamics is represented by a plane wave with a zero wave-vector. Then the trion-photon coupling is simplified:

$$\Omega_{\mathrm{T}}^{\pm}|_{\boldsymbol{B}=0} = \sqrt{n_{e,\pm\mathrm{K}}}\Omega\sqrt{S} \int \mathrm{d}^2\boldsymbol{r}\psi_{\mathrm{T}}(0, \boldsymbol{r}). \tag{27}$$

Analogously, the exciton-photon coupling reads[33]

$$\Omega_{\mathrm{X}} = \Omega \int \mathrm{d}^2\boldsymbol{r}\Psi_{\mathrm{X}}(\boldsymbol{r}, \boldsymbol{r}). \tag{28}$$

Note that similarly to the case of trions, the dynamics of center of mass cannot be decoupled from the internal dynamics if the magnetic field is present. In the absence of the magnetic field, one has $\Psi_{\mathrm{X}}(\boldsymbol{r}_e, \boldsymbol{r}_h) = \psi_{\mathrm{X}}(|\boldsymbol{r}_e - \boldsymbol{r}_h|)/\sqrt{S}$, where ψ_{X} is the wave function of relative dynamics involved in the well-known expression $\Omega_{\mathrm{X}} = \Omega\sqrt{S}\psi_{\mathrm{X}}(0)$[65].

Given the large energy separation (above 30 meV) between the exciton and trion optical transitions[28], we consider a strong coupling of trions and cavity modes *only*, i.e., we disregard the exciton resonance. The corresponding Hamiltonian reads

$$\hat{H}^{\pm} = \begin{pmatrix} \hbar\omega_{\mathrm{C}}^{\pm} & \Omega_{\mathrm{T}}^{\pm} \\ \Omega_{\mathrm{T}}^{\pm} & E_{\mathrm{T}}^{\pm} \end{pmatrix}, \tag{29}$$

where the superscript ± denotes circular polarization of the cavity mode and the trion valley index. The eigenmodes of this Hamiltonian correspond to the upper and lower trion-polaritons.

Data availability

Data sets generated during the current study are available from the corresponding author on reasonable request.

Received: 7 June 2024; Accepted: 12 November 2024;
Published online: 27 November 2024

References

1. Mak, K. F., Lee, C., Hone, J., Shan, J. & Heinz, T. F. Atomically thin MoS_2: a new direct-gap semiconductor. *Phys. Rev. Lett.* **105**, 136805 (2010).
2. Wang, G. et al. Colloquium: excitons in atomically thin transition metal dichalcogenides. *Rev. Mod. Phys.* **90**, 021001 (2018).
3. Chernikov, A. et al. Exciton Binding Energy and Nonhydrogenic Rydberg Series in Monolayer WS_2. *Phys. Rev. Lett.* **113**, 076802 (2014).
4. Rytova, N. S. The screened potential of a point charge in a thin film. *Moscow Univ. Phys. Bull.* **22**, 18 (1967).
5. Keldysh, L. V. Coulomb interaction in thin semiconductor and semimetal films. *JETP Lett.* **29**, 658 (1979).
6. Berkelbach, T. C., Hybertsen, M. S. & Reichman, D. R. Theory of neutral and charged excitons in monolayer transition metal dichalcogenides. *Phys. Rev. B* **88**, 045318 (2013).
7. Hüser, F., Olsen, T. & Thygesen, K. S. How dielectric screening in two-dimensional crystals affects the convergence of excited-state calculations: Monolayer MoS_2. *Phys. Rev. B* **88**, 245309 (2013).
8. Kormányos, A. et al. k· p theory for two-dimensional transition metal dichalcogenide semiconductors. *2D Mater.* **2**, 022001 (2015).
9. Srivastava, A. et al. Valley Zeeman effect in elementary optical excitations of monolayer WSe_2. *Nat. Phys.* **11**, 141–147 (2015).
10. Mostaani, E. et al. Diffusion quantum monte Carlo Study of excitonic complexes in two-dimensional transition-metal dichalcogenides. *Phys. Rev. B* **96**, 075431 (2017).
11. Mueller, T. & Malic, E. Exciton physics and device application of two-dimensional transition metal dichalcogenide semiconductors. *npj 2D Mater. Appl.* **2**, 29 (2018).
12. Anantharaman, S. B., Jo, K. & Jariwala, D. Exciton–photonics: from fundamental science to applications. *ACS nano* **15**, 12628–12654 (2021).
13. Ciarrocchi, A., Tagarelli, F., Avsar, A. & Kis, A. Excitonic devices with van der Waals heterostructures: valleytronics meets twistronics. *Nat. Rev. Mater.* **7**, 449–464 (2022).
14. Chernikov, A., Ruppert, C., Hill, H. M., Rigosi, A. F. & Heinz, T. F. Population inversion and giant bandgap renormalization in atomically thin WS_2 layers. *Nat. Photonics* **9**, 466–470 (2015).
15. Steinhoff, A. et al. Exciton fission in monolayer transition metal dichalcogenide semiconductors. *Nat. Commun.* **8**, 1166 (2017).
16. Estrecho, E. et al. Direct measurement of polariton-polariton interaction strength in the Thomas-Fermi regime of exciton-polariton condensation. *Phys. Rev. B* **100**, 035306 (2019).
17. Shahnazaryan, V., Iorsh, I., Shelykh, I. A. & Kyriienko, O. Exciton-exciton interaction in transition-metal dichalcogenide monolayers. *Phys. Rev. B* **96**, 115409 (2017).
18. Shahnazaryan, V., Kozin, V., Shelykh, I., Iorsh, I. & Kyriienko, O. Tunable optical nonlinearity for transition metal dichalcogenide polaritons dressed by a Fermi sea. *Phys. Rev. B* **102**, 115310 (2020).
19. Bleu, O., Li, G., Levinsen, J. & Parish, M. M. Polariton interactions in microcavities with atomically thin semiconductor layers. *Phys. Rev. Res.* **2**, 043185 (2020).
20. Fey, C., Schmelcher, P., Imamoglu, A. & Schmidt, R. Theory of exciton-electron scattering in atomically thin semiconductors. *Phys. Rev. B* **101**, 195417 (2020).
21. Erkensten, D., Brem, S. & Malic, E. Exciton-exciton interaction in transition metal dichalcogenide monolayers and van der Waals heterostructures. *Phys. Rev. B* **103**, 045426 (2021).
22. Cam, H. N., Phuc, N. T. & Osipov, V. A. Symmetry-dependent exciton-exciton interaction and intervalley biexciton in monolayer transition metal dichalcogenides. *npj 2D Mater. Appl.* **6**, 22 (2022).
23. Dufferwiel, S. et al. Exciton–polaritons in van der Waals heterostructures embedded in tunable microcavities. *Nat. Commun.* **6**, 8579 (2015).
24. Chernikov, A. et al. Electrical tuning of exciton binding energies in monolayer WS_2. *Phys. Rev. Lett.* **115**, 126802 (2015).
25. Mak, K. F. et al. Tightly bound trions in monolayer MoS_2. *Nat. Mater.* **12**, 207–211 (2013).
26. Ross, J. S. et al. Electrical control of neutral and charged excitons in a monolayer semiconductor. *Nat. Commun.* **4**, 1474 (2013).
27. Singh, A. et al. Trion formation dynamics in monolayer transition metal dichalcogenides. *Phys. Rev. B* **93**, 041401 (2016).
28. Courtade, E. et al. Charged excitons in monolayer WSe_2: experiment and theory. *Phys. Rev. B* **96**, 085302 (2017).
29. Sidler, M. et al. Fermi polaron-polaritons in charge-tunable atomically thin semiconductors. *Nat. Phys.* **13**, 255–261 (2017).
30. Efimkin, D. K. & MacDonald, A. H. Many-body theory of trion absorption features in two-dimensional semiconductors. *Phys. Rev. B* **95**, 035417 (2017).
31. Tan, L. B. et al. Interacting polaron-polaritons. *Phys. Rev. X* **10**, 021011 (2020).
32. Efimkin, D. K., Laird, E. K., Levinsen, J., Parish, M. M. & MacDonald, A. H. Electron-exciton interactions in the exciton-polaron problem. *Phys. Rev. B* **103**, 075417 (2021).
33. Glazov, M. M. Optical properties of charged excitons in two-dimensional semiconductors. *J. Chem. Phys.* **153**, 034703 (2020).
34. Dufferwiel, S. et al. Valley-addressable polaritons in atomically thin semiconductors. *Nat. Photonics* **11**, 497–501 (2017).

35. Zhumagulov, Y. V. et al. Microscopic theory of exciton and trion polaritons in doped monolayers of transition metal dichalcogenides. *npj Comput. Mater.* **8**, 92 (2022).
36. Emmanuele, R. et al. Highly nonlinear trion-polaritons in a monolayer semiconductor. *Nat. Commun.* **11**, 3589 (2020).
37. Kyriienko, O., Krizhanovskii, D. & Shelykh, I. Nonlinear quantum optics with trion polaritons in 2D monolayers: conventional and unconventional photon blockade. *Phys. Rev. Lett.* **125**, 197402 (2020).
38. Lyons, T. et al. Giant effective Zeeman splitting in a monolayer semiconductor realized by spin-selective strong light–matter coupling. *Nat. Photonics* **16**, 632–636 (2022).
39. Stier, A. V., McCreary, K. M., Jonker, B. T., Kono, J. & Crooker, S. A. Exciton diamagnetic shifts and valley Zeeman effects in monolayer WS_2 and MoS_2 to 65 tesla. *Nat. Commun.* **7**, 10643 (2016).
40. Stier, A. V. et al. Magnetooptics of Exciton Rydberg States in a Monolayer Semiconductor. *Phys. Rev. Lett.* **120**, 057405 (2018).
41. Goryca, M. et al. Revealing exciton masses and dielectric properties of monolayer semiconductors with high magnetic fields. *Nat. Commun.* **10**, 4172 (2019).
42. Have, J., Peres, N. & Pedersen, T. G. Excitonic magneto-optics in monolayer transition metal dichalcogenides: From nanoribbons to two-dimensional response. *Phys. Rev. B* **100**, 045411 (2019).
43. Liu, E. et al. Magnetophotoluminescence of exciton Rydberg states in monolayer WSe_2. *Phys. Rev. B* **99**, 205420 (2019).
44. Delhomme, A. et al. Magneto-spectroscopy of exciton Rydberg states in a CVD grown WSe_2 monolayer. *Appl. Phys. Lett.* **114**, 232104 (2019).
45. MacNeill, D. et al. Breaking of valley degeneracy by magnetic field in monolayer $MoSe_2$. *Phys. Rev. Lett.* **114**, 037401 (2015).
46. Klein, J. et al. Controlling exciton many-body states by the electric-field effect in monolayer MoS_2. *Phys. Rev. Res.* **3**, L022009 (2021).
47. Gor'kov, L. P. & Dzyaloshinskii, I. E. Contribution to the theory of the Mott exciton in a strong magnetic field. *JETP* **26**, 449 (1968).
48. Van der Donck, M., Zarenia, M. & Peeters, F. M. Excitons, trions, and biexcitons in transition-metal dichalcogenides: magnetic-field dependence. *Phys. Rev. B* **97**, 195408 (2018).
49. Förste, J. et al. Exciton g-factors in monolayer and bilayer WSe_2 from experiment and theory. *Nat. Commun.* **11**, 4539 (2020).
50. Na, M. & Rhee, S.-W. Electronic characterization of Al/PMMA[poly(methyl methacrylate)]/p-Si and Al/CEP(cyanoethyl pullulan)/p-Si structures. *Org. Electron.* **7**, 205–212 (2006).
51. Khestanova, E. et al. Electrostatic control of nonlinear photonic-crystal polaritons in a monolayer semiconductor. *Nano Lett*. **24**, 7350–7357 (2024).
52. Oreszczuk, K. et al. Enhancement of electron magnetic susceptibility due to many-body interactions in monolayer $MoSe_2$. *2D Mater.* **10**, 045019 (2023).
53. Lyons, T. P. et al. The valley Zeeman effect in inter-and intra-valley trions in monolayer WSe_2. *Nat. Commun.* **10**, 2330 (2019).
54. Wagner, K. et al. Autoionization and dressing of excited excitons by free carriers in monolayer WSe_2. *Phys. Rev. Lett.* **125**, 267401 (2020).
55. Varga, K. Solution of few-body problems with the stochastic variational method II: Two-dimensional systems. *Comput. Phys. Commun.* **179**, 591–596 (2008).
56. Kidd, D. W., Zhang, D. K. & Varga, K. Binding energies and structures of two-dimensional excitonic complexes in transition metal dichalcogenides. *Phys. Rev. B* **93**, 125423 (2016).
57. Varga, K. & Suzuki, Y. Solution of few-body problems with the stochastic variational method I. Central forces with zero orbital momentum. *Comput. Phys. Commun.* **106**, 157 (1997).
58. Suzuki, Y. & Varga, K. (eds.) *Stochastic variational approach to quantum-mechanical few-body problems* (Springer, 2014).
59. Varga, K. & Suzuki, Y. Precise solution of few-body problems with the stochastic variational method on a correlated Gaussian basis. *Phys. Rev. C* **52**, 2885 (1995).
60. Varga, K., Navratil, P., Usukura, J. & Suzuki, Y. Stochastic variational approach to few-electron artificial atoms. *Phys. Rev. B* **63**, 205308 (2001).
61. Yan, J. & Varga, K. Excited-state trions in two-dimensional materials. *Phys. Rev. B* **101**, 235435 (2020).
62. Lundt, N. et al. Room-temperature Tamm-plasmon exciton-polaritons with a WSe_2 monolayer. *Nat. Commun.* **7**, 13328 (2016).
63. Gu, J., Chakraborty, B., Khatoniar, M. & Menon, V. M. A room-temperature polariton light-emitting diode based on monolayer WS_2. *Nat. Nanotechnol.* **14**, 1024–1028 (2019).
64. Anton-Solanas, C. et al. Bosonic condensation of exciton–polaritons in an atomically thin crystal. *Nat. Mater.* **20**, 1233–1239 (2021).
65. Claudio Andreani, L. Optical transitions, excitons, and polaritons in bulk and low-dimensional semiconductor structures. in *Confined Electrons and photons: New physics and applications*, 57–112 (Springer, 1995).

Acknowledgements

The research is supported by the Ministry of Science and Higher Education of the Russian Federation (Goszadaniye) Project No. FSMG-2023-0011. V.S. acknowledges the support of 'Basis' Foundation (Project No. 22-1-3-43-1). The work of A.K. is supported by the Icelandic Research Fund (Rannís, Grant No.~2410550). The work of K.V. has been supported by the National Science Foundation (NSF) under Grant No. DMR-2217759.

Author contributions

V.S., A.K., Z.A., and I.S. developed the theoretical model. A.K. and K.V. developed the code for simulations. A.K. and I.A. performed the numerical simulations. V.S. managed the project. All the authors discussed the results and contributed to the preparation of the manuscript.

Competing interests

The authors declare no competing interests.

Additional information

Supplementary information The online version contains supplementary material available at https://doi.org/10.1038/s41699-024-00517-1.

Correspondence and requests for materials should be addressed to Vanik Shahnazaryan.